Cement and Concrete Research 42 (2012) 384–396

Contents lists available at SciVerse ScienceDirect

Cement and Concrete Research

journal homepage: http://ees.elsevier.com/CEMCON/default.asp

Effect of temperature on the water retention properties of two high performance concretes

Flore Brue [a,b,c,d,*], Catherine A. Davy [a,b,d], Frédéric Skoczylas [a,b,d], Nicolas Burlion [a,b,c], Xavier Bourbon [e]

[a] Université Lille Nord de France, F-59000 Lille, France
[b] LML, CNRS, UMR 8170, F-59650 Villeneuve d'Ascq, France
[c] Polytech'Lille, F-59650 Villeneuve d'Ascq, France
[d] EC Lille, LML, BP 48, F-59650 Villeneuve d'Ascq, France
[e] ANDRA, 1-7 rue Jean Monnet, 92298 Châtenay-Malabry Cedex, France

ARTICLE INFO

Article history:
Received 13 October 2010
Accepted 9 November 2011

Keywords:
High performance concrete (E)
Temperature (A)
Adsorption (C)
Waste management (E)
Radioactive waste (E)

ABSTRACT

This contribution aims at (1) determining experimentally the *first desorption isotherms* of two high performance concretes (based on CEM I and CEM V cements), at three different temperature levels $T = 20$, 50 and 80 °C, and (2) showing whether these may be simply described by adsorption and capillarity.
Results at 20 °C compare well with recently published results; in particular, an important desorption is observed at high *RH* (≥98%). A simple pore network model, based on Kelvin–Laplace's capillary theory, is implemented, and shows the existence of two main de-saturation modes, one at high pore radii (capillary pores), the other for pore radii on the order of a few nanometers (C-S-H porosity), where desorption is shown to occur. A complementary drying mechanism is evidenced at 80 °C, which is attributed to ettringite and/or C-S-H degradation. Finally, proper numerical fitting of all isotherm data is achieved using the well-known three-parameter BSB model.

1. Introduction

The French National Agency for Nuclear Waste Management (*Agence Nationale pour la gestion des Déchets RadioActifs*, Andra) is officially in charge of designing and assessing the feasibility, and the safety, of a long-term nuclear waste repository in deep geological medium. This assessment has to take into account the physical and chemical phenomena due to the waste activity, as well as processes in relation to the geological medium behavior [1]. In particular, the concrete components of the repository will be subjected to a de-saturation process, in relation to the facility building and exploitation (e.g. tunnel ventilation). The progressive closure of the repository is expected to stop this hydraulic process. Hence, Andra considers that concrete de-saturation would be partial, down to 50–60% relative humidity (*RH*). Moreover, an area of the repository aims at storing intermediate level wastes (ILW), which are exothermic: the maximum temperature in ILW vaults has been assessed as being close to 50 °C and, at worst, around 70–80 °C [1,2]. Therefore, identifying the effect of thermal loading on the de-saturation process is critical for the design of the French repository.

1.1. Temperature and saturation state

At constant temperature, a sorption (or desorption) isotherm is the tool, which relates the water saturation state of a porous material to the relative humidity of the surrounding air. In this study, following Andra's recommendations, we solely reproduce a de-saturation process, which corresponds to the first desorption from an initially fully water-saturated state, yet under temperature (up to 80 °C). As S. Poyet recalls [2], although the first sorption and the subsequent desorption/sorption isotherms are hardly sensitive to temperature change (up to 60 °C at least), the *first desorption* isotherm is greatly modified by temperature increase [2–4].

In the literature, to our knowledge, few studies relate to the influence of temperature on the first desorption isotherm, for temperatures lower than 100 °C; comparison between different materials (subjected to identical de-saturation conditions) is also scarce. Available studies show a significant change in shape of the *first desorption* curves with temperature [2–5]. It is evidence of the actual influence of temperature on the physical mechanisms involved during a de-saturation process. Usually, such temperature dependence in the sorption properties of cement-based materials is attributed to the evolution of water properties [5–9], together with the coarsening of the pore structure (due to ettringite dissolution and calcium silicate hydrates (C-S-H) alteration) [2,6]. Quite controversially, S. Poyet et al. [10] provide experimental and numerical elements, which support that the main phenomenon at work is solely thermal desorption, up to 80 °C.

* Corresponding author at: EC Lille, LML, BP 48, F-59650 Villeneuve d'Ascq, France.
E-mail address: flore.brue@ec-lille.fr (F. Brue).

0008-8846/$ – see front matter © 2011 Elsevier Ltd. All rights reserved.
doi:10.1016/j.cemconres.2011.11.005

1.2. Physical phenomena involved during de-saturation

The study of desorption isotherms refers to potentially coexisting physical mechanisms, related to water retention within the material pore network: these are mainly capillarity and desorption/adsorption [11].

The capillary theory is based on the analysis of water chemical potential [11–14]. Kelvin–Laplace's equation applied to water allows the calculation of the smallest drained diameter d^i at given temperature T and for given humidity conditions, as:

$$d^i = -\frac{4\gamma_w(T)M_w}{\Re T\rho_w(T)\ln(RH)} \quad (1)$$

where ρ_w is water specific mass (function of temperature T) [kg/m^3]; $\Re$ is the perfect gas constant [J/mol·K]; T is temperature [K]; M_w is water molar mass [kg/mol] and γ_w is the surface tension of water/air (also a function of temperature) [7]. Capillary condensation/evaporation is also associated to hysteresis loops, which shapes have been classified, e.g. IUPAC classification [15]. As detailed above, hysteresis in sorption isotherms is not the focus of this paper, despite its well-known existence for cement-based materials [16,17]. Rather, a *specific* description is sought for the first desorption isotherm solely, which accounts for temperature dependence.

Adsorption is an exothermic process, and as such, temperature increase is bound to hinder adsorption and promote desorption instead [2]. Different models have been developed to relate the sorption isotherm to water retention mechanisms and to temperature, based on the adsorption theory [11,16,18,19]. The BET model (*for Brunauer, Emmet & Teller* [20]) reproduces the first monolayer of water adsorbing on pore surfaces, so that its *RH* validity domain to fit desorption isotherms is below 30–50% at ambient temperature [20]. In order to account for multi-layer adsorption, occurring at higher *RH*, the BSB model (*for Brunauer, Skalny & Bodor*) [13,18,21,22] was derived from the BET model. It is also known as the three-parameter BET model, or as the GAB model (*for Guggenheim, Anderson & Boer*) [2,14,18], and it has proven proper suitability to describe the first desorption isotherm of varied concretes [10,18,22]. While the BET model considers only the lowest relative humidities, the BSB model covers almost the full *RH*-range at ambient temperature, with reliable predictions between 5 and 95% [12,18,19,22]. The BSB model writes:

$$w(RH) = \frac{C \times k \times w_m \times RH}{(1-k \times RH)[1+(C-1)k \times RH]} \quad (2)$$

$w(RH)$ is the water content (expressed in mass%) at given *RH*-value, C, k and w_m are the model parameters to be identified depending on the material considered and on temperature T. For $k=1$, one recovers the BET model. Physical interpretation of these parameters is provided in [18], see also Section 4.2.2 hereafter.

While the BET and BSB models account for adsorption phenomena, which makes them suitable to describe first desorption isotherms, they are not adapted to two cases: (1) occurrence of hysteresis loops, as observed on cement-based materials [16,17]; (2) high *RH* values (≥95%) [19].

1.3. Aims and scopes

Our aim is to assess first desorption isotherms under temperature for *two* industrial concretes based on CEM I and CEM V/A-type cements (European standard denominations). An originality of this work is to perform desorption on initially 6 month-mature samples, de-saturated *each* from the fully-saturated state down to 12%*RH*, instead of using different samples at each *RH*, as it is usually done [2,17,23].

Firstly, our experimental data are compared to former studies [2,17,23]. Desorption results are then related to concrete microstructure using porosity, pore size distribution and gas permeability measurements. Finally, we discuss whether the first desorption isotherms of both concretes under temperature may be simply described by adsorption and capillarity, with minor influence of other phenomena, such as solid phase alteration (ettringite or C-S-H) [2].

2. Experimental approach

2.1. Materials

Both materials studied here are considered as 'reference concretes' in Andra's program for disposal design. Two types of cement are used: (1) a CEM I type, which is made of pure Portland cement, and (2) a CEM V/A type, which is constituted of 60% clinker in mass, 22% blast-furnace slag, 14% fly ash and 4% setting regulator, according to NF EN 196-4 European Standard [24,25]. Concrete made with CEM I cement has a water-to-cement ratio (W/C) equal to 0.43: it is referred to as 'CEM I'. Concrete prepared with CEM V/A cement has a (W/C) ratio equal to 0.39: it is referred to as 'CEM V'. Table 1 presents the formulation of both concretes. The difference between both mature materials is the microstructure, i.e. both solid phases and pore network morphology, which have a major impact on transfer properties. In particular, CEM V/A type cement is bound to promote pozzolanic reactions, i.e. delayed C-S-H formation by consumption of initially formed portlandite.

2.1.1. Mixing and maturation

All samples are made from a single batch for each cement type. After mixing, each batch is poured into 4 beam forms with a section of (15×15) cm^2 and a length of 1 m. Desiccation is avoided by protecting the upper beam surface by plastic sheets. After un-molding at 5 days, both concretes are cured in lime-saturated water, at 20 °C for six months. Due to this, we consider that the hydration process is sufficiently advanced, so that concrete microstructure will no longer vary significantly [2,16,26]. In support to this, Table 2 shows that the average mass intake of CEM I concrete is 6 times greater during the first 6 month maturation rather than during the

Table 1
Concrete formulations.

Concrete name	CEM I			CEM V		
Component	Nature	Source	Quantity [kg/m^3]	Nature	Source	Quantity [kg/m^3]
Cement	CEM I 52.5 R	Lafarge, France	400	CEM V/A 42.5 N	Calcia, France	450
Sand	Limestone [0–4 mm]	Boulonnais quarry, France	858	Limestone [0–4 mm]	Boulonnais quarry, France	800
Gravel	Limestone [5–12 mm]	Boulonnais quarry, France	945	Limestone [5–12 mm]	Boulonnais quarry, France	984
Superplasticizer	Glenium 27	BASF	10	Glenium 27	BASF	11.5
Water	–	–	171	–	–	176.3
W/C	0.43			0.39		

Table 2
Water intake after 6 months and 3 years maturation.

	CEM I	CEM V
Water intake after 6 month maturation [%]	Average = +0.8% Min value = +0.5% Max value = +1.15%	Average = +1.15% Min value = +0.85% Max value = +1.42%
Water intake between 6 months and 3 years [%]	Average = +0.12% Min value = +0.1% Max value = +0.155%	Average = +0.33% Min value = +0.254% Max value = +0.386%
Ratio of average values	0.8/0.12 = 6.66	1.15/0.33 = 3.48

subsequent 3 years; the same ratio for CEM V concrete is above 3. Also, as detailed by [18], after 6 months curing, the effect of age upon desorption isotherms may be neglected without significant loss of accuracy. Concrete samples are assumed fully water-saturated at the end of this period.

2.1.2. Sample manufacturing

During maturation, cylindrical samples (Ø = 37.5 mm) are cored from the beams, and then, cut to a height h equal to 50 mm for desaturation experiments (and 75 mm for mechanical compressive tests); both coring and cutting are performed under water, so that it is assumed that all samples remain fully water-saturated; after manufacturing, samples are kept in lime-saturated water at 20 °C until 6 month maturation. The chosen sample size is sufficiently large to ensure their representativeness with regard to the representative elementary volume (R.E.V. = 1104 mm^3 and biggest aggregate diameter 12 mm), but small enough to limit the time needed to reach hydrous equilibrium [2,16]. Several prismatic samples ($4\times4\times16 cm^3$) are also made, in order to check whether porosity measurements are sensitive to sample size. Fig. 1 provides a detailed overview of the experimental approach, which is detailed in the next sections.

2.1.3. Initial characterization of materials

Uniaxial compressive strength, gas permeability, total connected porosity and pore size distribution are characterized for each material:

- Uniaxial compressive strength is characterized after 6 month maturation, in the fully water saturated state, as the peak stress sustained by 2 (Ø = 37.5 mm, h = 75 mm) cylinders for each formulation.
- Gas permeability of each concrete is measured on dried material (obtained by oven-drying at 60 °C until constant weight) by using an inert gas (argon), and by placing the sample in a triaxial cell with a confining pressure P_{conf} = 5 MPa: this value is required by the measurement methodology in order to limit the potential influence of drying-induced micro-cracks; also, it corresponds to lower bound values of the in situ loading [27]. Apparent permeabilities are measured as a function of gas injection pressure. Evaluation of the Klinkenberg effect allows the calculation of the material intrinsic gas permeability [28].
- The mean difference in mass between water-saturated and dry states provides an estimation of the total porosity for each concrete [29]. In order to check the influence of the drying temperature on this measurement, two values are chosen for the dry state: 60 °C and 105 °C: a moderate drying at 60 °C allows the drainage of porosity down to C-S-H gel pores [30], while drying at 105 °C leads to a complete drainage together with the apparition of micro-cracking, and potential small solid phase alterations [30,31]. For each concrete, the measurement of connected porosity at 60 °C is made on 48 cylindrical samples of diameter Ø = 37.5 mm (h = 50 mm for 24 samples, and h = 75 mm for 24 samples) and 3 prismatic samples with a volume equal to $(4\times4\times16)$ cm^3. For both concretes, no significant influence of sample size is observed. Therefore, porosity after oven-drying at 105 °C is measured on four cylindrical samples (Ø = 37.5 mm and h = 20 mm) only.
- Pore size distribution is measured by Mercury Intrusion Porosimetry (MIP) on one concrete sample (of a volume of less than 1 cm^3) in the dry state (after oven-drying at 60 °C) using mercury pressures of up to 200 MPa. Each sample is carefully chosen in order to avoid containing big aggregates, but rather cement paste. This test is able to characterize a proportion of pores with radii between 6 nm and 400 μm.

2.2. Control of the desorption process

Desorption is performed at three fixed temperatures T (20 °C, 50 °C and 80 °C). 20 °C represents the reference temperature; 50 °C

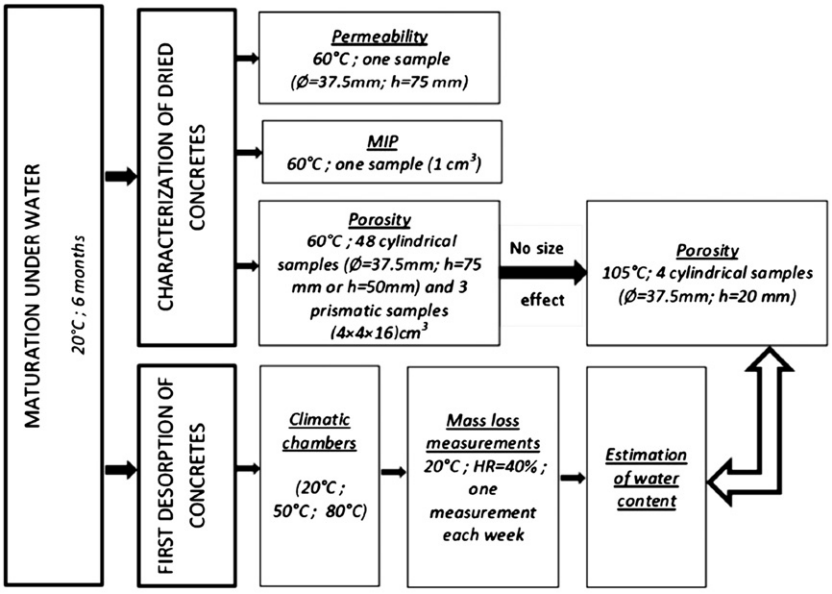

Fig. 1. Schematic representation of our experimental approach.

is the standard operating temperature for exothermic ILW, whereas 80 °C is the extreme temperature of the study (peak value). Temperature and relative humidity are both controlled by the use of climatic chambers. A fixed relative humidity *RH* is imposed at successive values *RH* = [98%; 90%; 80%; 70%; 60%; 50%; 30%; 12%]. All measurements are carried out on four cylindrical samples at each temperature and for each concrete.

In order to estimate water content *w* at each *RH*-value, sample mass variation is measured within less than half an hour, under controlled conditions ($T = 20 \pm 1$ °C and $RH = 40 \pm 5\%$) with an accuracy of ± 0.01 g. Each time a new *RH*-value is imposed, mass is recorded every two days during the first two weeks, and then each week until mass stabilization, in order to limit destabilization of the climatic chamber atmosphere. Moreover, from $RH = 80\%$ and lower, nitrogen is added in the climatic chamber after each measurement, in order to prevent carbonation, which is maximal for *RH* between 65 and 70% [32]. At each *RH*-step, once the change between three consecutive measurements (i.e. during three successive weeks) is less than $\pm 0.1\%$, thermodynamic equilibrium is assumed to be reached: this occurs after at least two months under the prescribed *RH*. Consequently, water content *w* (%) is determined as:

$$w = \frac{m - m_{dry}}{m_{dry}} \tag{3}$$

where *m* is the current mass at a considered *RH*-value and m_{dry} is the dry sample mass. For all samples, m_{dry} is deduced from total connected porosity ϕ assessed at 105 °C (see the next section for the explanation of this choice of temperature). Indeed, samples used for desorption isotherms have not been dried before the experiment: their initial state is 6 month maturation under lime-saturated water, assumed to correspond to full water saturation. To date, despite *five year testing*, these samples have not reached full equilibrium at $T = 20$ or 50 °C *and* $RH < 50\%$, i.e. no dry state yet. On the opposite, thermodynamic equilibrium has been obtained at $T = 80$ °C, down to $RH = 12\%$.

2.2.1. Dry and saturated states

The choice of reference dry and saturated states is essential for the estimation of water content. The saturated state of samples is assumed obtained at the end of 6 month maturation under water. The reference dry state is chosen after drying in an oven at 105 °C until constant weight. Such drying leads to small thermal micro-cracking and to changes in the microstructure of the hydrates [30,33]. However, no significant effect on gas permeability and total connected porosity has been observed on model mortars [31]. As the maximum temperature used for the desorption experiments is of 80 °C, it was found more adequate to select a higher oven-drying temperature of 105 °C as the reference dry state.

Dry mass m_{dry}, necessary for water content *w* assessment (see Eq. (3)), is derived by a proportionality rule from samples used for porosity assessment, as follows. From ($\varnothing = 37.5$ mm; $h = 20$ mm) samples oven-dried at 105 °C, an average water mass proportion is deduced as:

$$\%mass = \frac{M_{sat} - M_{dry}}{M_{sat}} \tag{4.1}$$

where M_{sat} and M_{dry} are average water-saturated and dry masses. For CEMV, $\%mass = 4.8\%$, and for CEMI, $\%mass = 3.3\%$. This parameter is assumed independent of sample size and of temperature *T*, when it is used on de-saturation ($\varnothing = 37.5$ mm; $h = 50$ mm) samples to assess dry mass m_{dry}, by a simple rule of proportionality:

$$m_{dry} = (1 - \%mass) m_{sat} \tag{4.2}$$

where m_{sat} is sample saturated mass (at 6 month maturation), measured at 20 °C after surface drying with a clean tissue. Water density variation between 20 °C and 80 °C is of 2%: water density is of 0.99 at 20 °C, down to 0.97 at 80 °C, so that m_{sat} is not significantly different for our isotherm temperatures. At present date, CEMI and CEMV de-saturation samples are stabilized at $T = 80$ °C and $RH = 12\%$: this provides *actual* average dry mass values at 136.48 g (+/−0.86 g) for CEMI and 127.13 g (+/−0.88 g) for CEMV. With Eq. (4.2), m_{dry} is of 137.90 g for CEMI and 129.05 g for CEMV. Therefore, m_{dry} represents a relative difference of 1% for CEMI and of 1.5% for CEMV, when compared with actual dry mass: this validates very satisfactorily the method chosen to assess *w* at any temperature *T*, whatever the material considered.

2.3. Comparison between different material batches

As mentioned in Section 1, sorption phenomena have been investigated by other authors, for concrete formulations identical to those used here: despite varying experimental conditions and different research objectives, this allows a useful comparison from one material batch to another (see Sections 3 and 4).

For a *single* concrete with an identical formulation to our so-called 'CEM I' concrete (see Section 2.1), S. Poyet [2] determines experimentally first desorption isotherms at temperatures *T* of 30 and 80 °C, after more than one year maturation. Each *RH* value is prescribed by a salt-saturated solution, and desorption tests are performed on *different* samples per *RH*; no comparison with other concretes is proposed. Also, recent publication by Ranaivomanana et al. [17] compares first desorption isotherms at 20 °C, down to 60%*RH* only, for two concretes with identical formulation to ours, after one year curing; as in [2], *different* samples are used at each *RH* value. In our laboratory, W. Chen [23] has determined full sorption/desorption isotherms of 6 months mature CEM I and CEM V concretes at 20 °C, by using salt saturated solutions and *different* samples per *RH* value. As in [2,17], the batches used in [23] are different from those used here.

3. Experimental results

3.1. Preliminary results: strength and microstructure

Preliminary characterization results are presented in Table 3.

Uniaxial compressive strength f_c of both materials, at 6 month maturation, supports their classification as *high performance concretes*: f_c (saturated state) ≥ 60 MPa.

3.1.1. Pore microstructure assessment

For both concretes, connected porosity ϕ presents limited scatter, after oven-drying at 60 or 105 °C. In particular, connected porosity ϕ of 60 °C oven-dried CEM I concrete is 8.1% on average, with a standard deviation of 0.9 (i.e. 11% of the average); for 60 °C oven-dried CEM V concrete, ϕ is 11.9% on average, with a standard deviation limited to 0.7 (i.e. 5.9% of the average). Although CEM I concrete is less porous than CEM V (either after 60 °C or 105 °C oven-drying), it has lower strength

Table 3
Intrinsic gas permeability at $P_{conf} = 5$ MPa, total porosity (water saturation method followed by oven-drying at either 60 or 105 °C) and strength of fully water-saturated concretes, measured at 6 month maturation.

Property	Unit	CEM I	CEM V
Permeability K	m^2	5.10^{-18}	2.10^{-18}
Porosity ϕ (60 °C) +/− standard deviation	%	8.1 +/− 0.9	11.9 +/− 0.7
Porosity ϕ (105 °C) +/− standard deviation	%	10.1 +/− 0.7	15.3 +/− 0.4
Compressive strength f_c (saturated state) +/− mean deviation	MPa	60 +/− 2	78 +/− 3

and greater permeability than CEM V, see Table 3. This illustrates significant differences in the arrangement of their pore microstructure.

In a similar way for both concretes, pore size distributions obtained by MIP (Fig. 2) present three distinct peaks: one is located between 1 and 2 μm, which is attributed to large capillary pores, entrapped air bubbles and/or to micro-cracks (potentially due to sample oven-drying) [17]; the second, much smaller, peak is located between 100 nm and 1 μm: it is centered around 200 nm for CEM I and 400 nm for CEM V, and corresponds to capillary pores [34]; the third, greatest peak is centered around 30 nm for CEM I and 40 nm for CEM V. As a matter of comparison, recent analysis by NMR on fully water-saturated cement paste [35] indicates the presence of two populations of nano-pores: one is in the 2–5 nm range, which is interpreted as C-S-H porosity (intra-layer pores); the other is in the 14–30 nm range, which corresponds to the second peak observed by MIP on our concretes. The latter is attributed to pores located in non-crystalline areas, between C-S-H layers (inter-layer pores). The main difference between CEM I and CEM V concretes lies at the left end of the MIP pore size distribution: at a diameter of 6 nm (which is the lowest measurable by MIP), CEM V presents a cumulated intruded volume of 0.018 ml/g (with a slope increasing towards lower radii), whereas that of CEM I is equal to 0.002 ml/g only (with a decreasing slope towards lower radii), i.e. CEM V concrete seems to have significantly more of the narrowest gel pores of C-S-H, than CEM I. This difference is attributed to pozzolanic additions in CEM V/A-type cement, which lead to the formation of a greater amount of C-S-H than in CEM I.

In support to this, numerical simulations in [17] provide 0.098 m^3 C-S-H/m^3 for CEM I concrete, and 0.115 m^3 C-S-H/m^3 for CEM V concrete. Different numerical simulations, and sorption experiments on CEM I and CEM V pastes by [36] (based on [37]) also support the presence of a greater C-S-H amount in CEM V than in CEM I. C-S-H having finer pores than other constituents of the microstructure, CEM V concrete has a finer porosity than CEM I, even if its total porosity is higher [17,38–40]. This argument is also supported by gas permeability, which is divided by two when comparing CEM I to CEM V, see Table 3. Finally, using desorption isotherm results in [23], the specific surface (S_{BET}) of each concrete is estimated with the BET model [2,11,16,18] in a *RH*-range between 11% and 43%. It was found that S_{BET} (*CEM I*) = 18 m^2/g and S_{BET} (*CEM V*) = 20 m^2/g. Also, our MIP tests provide S_{BET} (*CEM I*) = 2.35 m^2/g and S_{BET} (*CEM V*) = 4.88 m^2/g, showing the same tendency between both concretes: the specific surface is higher for CEM V than for CEM I. This is further evidence that the CEM V microstructure includes a greater C-S-H amount than CEM I, which means a finer porosity.

3.1.2. Microstructure comparison with other concrete batches

These microstructural features may be usefully compared to those of S. Poyet [2] on CEM I concrete, and to those of H. Ranaivomanana et al. [17] and W. Chen [23] on both CEM I and CEM V concretes: their materials are manufactured with identical formulation to ours, so that material variability may be assessed from one batch to another.

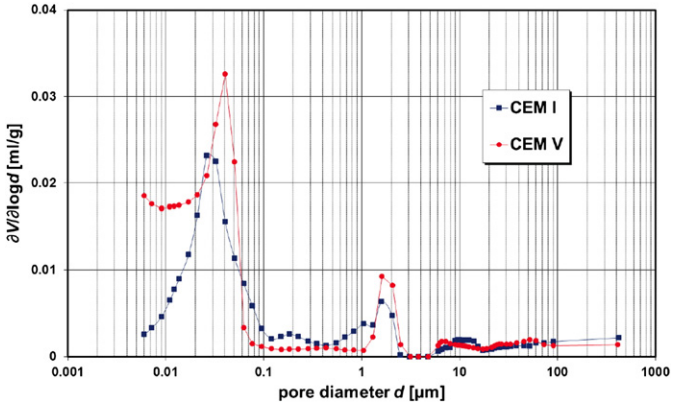

Fig. 2. Porosity distribution of CEM I and CEM V concretes measured by mercury intrusion porosimetry (MIP).

For CEM I concrete, after one year water-curing and 60 °C oven-drying, S. Poyet [2] measures an intrinsic gas permeability of 2×10^{-17} m^2 (average on three samples) under nitrogen flow. This value is four times greater than our value of 5×10^{-18} m^2. Indeed, Poyet's values are obtained under low sample confinement, which is insufficient to close up micro-cracks and decrease permeability, as with our 5 MPa confinement. S. Poyet [2] also measures greater connected porosity than ours after drying at 60 and 105 °C, with values at 11.3% and 12.3% respectively (to compare to our values of 8.1 and 10.1%). Pore size distributions in S. Poyet [2] show that the second (smaller) peak pore size ranges from 80 nm up to 150 nm, for samples tested at a maximum temperature of 30 °C, whereas our peak pore size value is at 40 nm only. All these results (gas permeability, porosity and MIP) show that despite an identical formulation, the microstructure of the CEM I concrete batch presented in S. Poyet [2] has significantly bigger pores, and bigger porosity, than our batch. Together with the different test protocols, this should be kept in mind when comparing desorption isotherms between both studies.

As for H. Ranaivomanana et al. [17], after one year water curing and 105 °C oven-drying, CEM I concrete porosity is of 12.3% (for which we have a lower value of 10.1%); CEM V concrete porosity is of 14.7%, for which we have assessed a slightly greater value of 15.3% +/− 0.4. By inverse analysis, both concretes are attributed peak pore sizes at 1.5 nm (C-S-H gel pores), 9.5 nm (inter-layer pores), and 410 nm (CEM I) or 580 nm (CEM V). These latter values are one order of magnitude greater than our MIP measurements. Under low confinement (of 0.1 to 0.4 MPa), intrinsic gas permeability is 4.0×10^{-17} m^2 for CEM I concrete, and 5.5×10^{-17} m^2 for CEM V. This is the opposite to our observations of greater permeability for CEM I than for CEM V concrete. Again, this difference is attributed to our 5 MPa confinement, which closes up a number of micro-cracks created by oven-drying: in our study, gas permeability is assessed with limited micro-crack influence.

In W. Chen [23], after 65 °C oven-drying of 9 samples per material, porosity is 8.3% +/− 0.4 for CEM I (we have a very close 8.1% +/− 0.9) and 10.3% +/− 0.6 for CEM V (we have a significantly greater 11.9% +/− 0.7).

It is concluded that differences in material manufacturing lead to significant divergence in the pore microstructure of mature concretes, which are bound to impact sorption isotherms.

3.2. First desorption isotherms

All experimental curves presented in Figs. 3, 4 and 5 are averages: scattering is shown using error bars, which represent the min/max values. Figs. 3 and 4 show the evolution of the average mass loss, for CEM I and CEM V concretes respectively. Fig. 5 presents the first desorption isotherms of both materials in terms of water content *w* (%) vs. *RH* and temperature *T*. Isotherms are deduced from stabilized mass variation values at each *RH* (see Figs. 3 and 4).

3.2.1. Kinetics and mass loss amplitude

For each concrete analyzed individually, Figs. 3 and 4 show that the effect of temperature *T* is double: first, on the water retention kinetics and secondly, on the relative mass loss amplitude. For instance, for both concretes, mass stabilization at *RH* = 50% is obtained after a total of 1081 days at 80 °C, whereas it has still not occurred at 20 and 50 °C after more than 1400 days experiment. The 50%-*RH* step at 20 °C and 50 °C is not ended yet.

➢ The increase in water retention kinetics is attributed to three main causes: (1) the decrease in water viscosity and in water/air surface tension with temperature *T* [3,7], (2) the local increase in

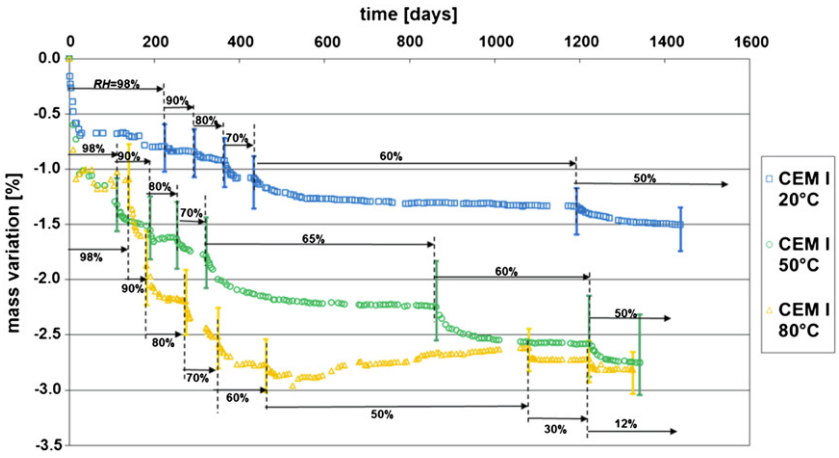

Fig. 3. Mass variation of CEM I concrete vs. temperature T and RH (%).

saturated water vapor pressure (P_{vap}^{sat}) with T [6], and (3) the increase in desorption with temperature [2,3]. This analysis would require further validation, yet it is not the focus of this paper.

➢ In first instance, the greater mass loss amplitude with temperature is attributed to (1) a greater amount of drained pores, in relation with the decrease in smallest drained diameter with temperature T increase, see Table 4, and (2) a smaller thickness of adsorbed water on pore walls when T increases [2]. Each phenomenon may be accounted for by Kelvin–Laplace's law or by the BSB model (see Sections 1 and 4).

One notices that, for CEM I at 80 °C and $RH = 50\%$, mass evolution presents an unexpected increase. The first possible cause would be carbonation, in spite of nitrogen introduction in the climatic chambers after each measurement. However, test made with phenolphthalein does not show the presence of a carbonation front. Rather, a temporary fault in the climatic chamber regulation might be responsible for this, although a $RH = 50\% +/- 1$ was regularly recorded by placing an independent thermo-hygrometer inside the climatic chamber. As further RH-steps lead to a stabilization in mass variation, results for CEM I concrete at 80 °C are kept at $RH = 50\%$ and below, yet they should be considered with some caution (see Section 4).

3.2.2. Desorption isotherms at high RH

Let us now consider the corresponding desorption isotherms, see Fig. 5. Firstly, for both concretes, a strong fall in the isotherm is observed between RH = 100 and 98%, which increases with temperature T. At 20 °C, for CEM I concrete, the porosity associated with these percolated pores represents 21% of the total open porosity (it amounts to 31% at 80 °C); at 20 °C also, for CEM V concrete, it constitutes 4% of the total porosity (it amounts to 15% at 80 °C). At 20 °C, this saturation fall is also accounted for in the literature on mature cement pastes [36,41], and by H. Ranaivomanana et al. [17] and W. Chen [23] for CEM I and CEM V concretes, see Figs. 6 and 7, where the isotherms are expressed in terms of water saturation level:

$$S_w = \frac{m(RH) - m_{dry}}{m_{saturated} - m_{dry}} \quad (5)$$

vs. RH. The strong decrease in S_w at $RH = 98\%$ is of similar value in our study and in H. Ranaivomanana et al. [17] for CEM I concrete, whereas it is significantly greater in H. Ranaivomanana et al. [17] for CEM V concrete. Therefore, observing a strong fall in the isotherm at high RH is independent of the material batch and nature: one is recorded whatever the concrete and the study, the main difference being in the extent of water loss. Also, the strong fall in the isotherm does not significantly depend on sample size: these are different in [17] and here, yet the decrease in S_w is similar for CEM I at 20 °C.

The observations of a greater mass loss for CEM I concrete than CEM V at high RH are consistent with a greater amount of coarse pores for CEM I than CEM V, as follows. At $RH = 98\%$, Kelvin–Laplace's law at 20 °C (resp. 50 and 80 °C) predicts that pores of diameter d^i larger than 106 nm (resp. 91 nm and 78 nm) are de-saturated, see Table 4. This assumes that all pores larger than d^i are fully accessible to air [42]. MIP results in Fig. 2 show that, at 20 °C, this corresponds to pores below the first peak located between 1 and 2 μm, which is

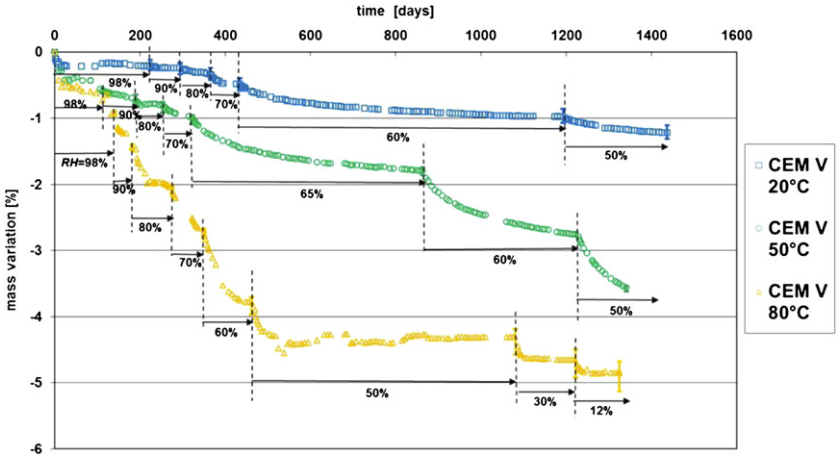

Fig. 4. Mass variation of CEM V concrete vs. temperature T and RH (%).

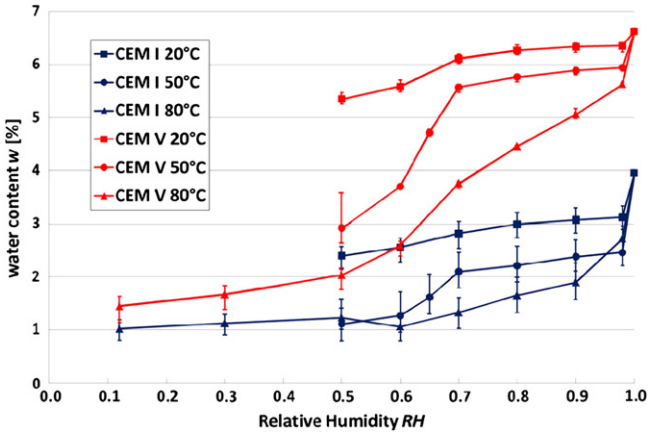

Fig. 5. First desorption isotherms expressed as water content w (%) vs. RH (%), for both concretes and at temperature $T = 20$, 50 and 80 °C, for $12\% \leq RH \leq 100\%$.

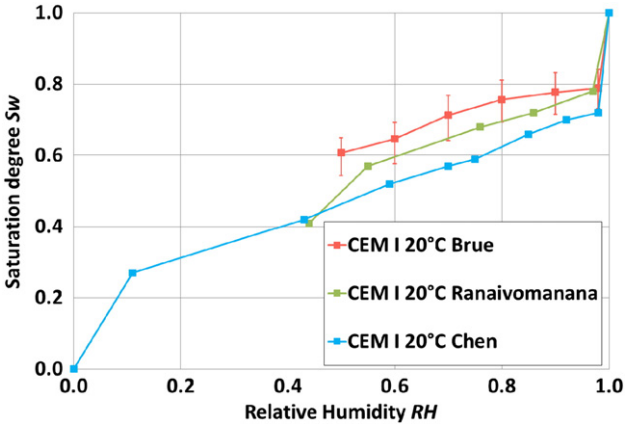

Fig. 6. Comparison of first desorption isotherms (saturation degree S_w vs. RH) for three different batches of CEM I concrete, from this study (labeled 'Brue'), Ref. [23] (labeled 'Chen') and Ref. [17] (labeled 'Ranaivomanana') at 20 °C.

attributed to entrapped air bubbles, large capillary pores or to micro-cracks, see Section 3.1 and [17]. As H. Ranaivomanana et al. [17] propose, this percolating pore network, which drains very quickly when RH decreases, may be constituted of wide interconnected pores, or of large pores connected by micro-cracks. Such micro-cracks would be due to concrete shrinkage during maturation under water. At 20 °C, the total volume of pores bigger than 106 nm corresponds to the area under the MIP curves in the [106 nm–400 μm] pore diameter range, see Fig. 2: this area is clearly greater for CEM I than CEM V, which justifies that CEM I concrete drains more than CEM V at $RH = 98\%$.

3.2.3. Desorption isotherms: effect of temperature

The effect of temperature for each concrete considered individually is assessed from results presented in Fig.5.

For each concrete, below $RH = 98\%$, the greater the temperature, the lower the water retention ability. More precisely, at $T = 50$ °C and RH in the range [70–98]%, the slope of the isotherm is similar to that at 20 °C. For RH lower than 70%, the slope of the isotherm at 50 °C is significantly greater than at 20 °C. This means that significant thermal activation is observed for $RH \leq 70\%$.

For CEM V, the slope of the isotherm is greater at $T = 80$ °C than at 20 or 50 °C whatever $RH \leq 98\%$: at 80 °C, thermally activated desorption is observed whatever the RH.

For CEM I, the slope of the isotherm is greater at $T = 80$ °C than at 20 or 50 °C, down to $RH = 60\%$. Below $RH = 60\%$, a stabilization in water content is observed, at very low values on the order of 1%.

3.2.4. Desorption isotherms: influence of cement type

At given temperature T, water retention properties are also compared in terms of cement type, i.e. in relation to concrete microstructure, see Fig. 5 again. First, the initial water content, at $RH = 100\%$, is greater for CEM V concrete ($w(RH = 100\%) = 6.63\%$) than for CEM I ($w(RH = 100\%) = 3.95\%$). This is attributed to CEM V greater porosity than CEM I. On the opposite, the initial drop in water content (for RH between 100% and 98%) is higher for CEM I than for CEM V, which is associated to a greater amount of coarser pores in CEM I, see previous paragraph.

At RH lower than 98%, for CEM V, a greater slope in the isotherm is recorded than for CEM I, from $RH = 70\%$ at 20 °C and 50 °C and most significantly, from $RH = 90\%$ at 80 °C. From these RH values, the drained pore diameter d^i is on the order of about ten nanometers at most, see Table 4, which corresponds to C-S-H gel inter- and intra-porosity [12,35]. Observing a greater desorption slope is consistent with the fact that CEM V concrete has more of these C-S-H pores (see Section 3.1 and [17,36,38–40]).

This is also observed on the first desorption isotherms of CEM I and CEM V concretes at 20 °C by W. Chen [23] and H. Ranaivomanana et al. [17], see Figs. 6 and 7: CEM V concrete remains more saturated than CEM I over the tested RH range (from 98 down to 11% for [23]), meaning that its water retention ability is greater over a wide RH range.

Table 4
Smallest drained diameter d^i as a function of relative humidity RH, obtained using Kelvin–Laplace's law at temperature T = 20, 50 or 80 °C.

Relative humidity RH [–]	d^i 20 °C [nm]	d^i 50 °C [nm]	d^i 80 °C [nm]
0.98	106.56	91.22	78.29
0.9	20.43	17.49	15.01
0.8	9.65	8.26	7.09
0.7	6.04	5.17	4.43
0.6	4.21	3.61	3.1
0.5	3.11	2.66	2.28
0.3	1.79	1.53	1.31
0.12	1.02	0.87	0.75
0.05	0.72	0.62	0.53

3.2.5. Desorption isotherms: effect of concrete batch

Comparison with W. Chen [23] and H. Ranaivomanana et al. [17] has been detailed above. As for S. Poyet [2], when comparing his results for CEM I with ours, one notes several differences. A significantly lower fall in water content is obtained by [2] at high RH and 80 °C, see

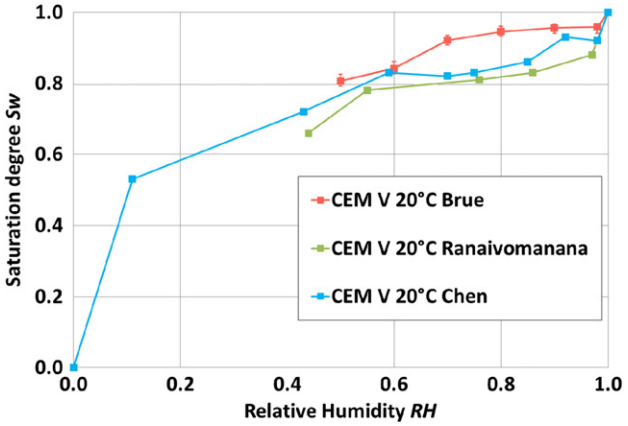

Fig. 7. Comparison of first desorption isotherms (saturation degree S_w vs. RH) for three different batches of CEM V concrete, from this study (labeled 'Brue'), Ref. [23] (labeled 'Chen') and Ref. [17] (labeled 'Ranaivomanana') at 20 °C.

Fig. 8. Moreover, no significant fall at high *RH* is observed on the 30 °C isotherm.

Also, the shape of the isotherm at 30 °C by S. Poyet [2] and that for our batch at 20 °C are clearly very different, with a much greater desorption slope in the case of [2]: it is of ca. 0.52 g/10%*RH*, as compared to a slope of ca. 0.1 g/10%*RH* for our CEM I batch in the range 50–98% *RH*.

At 80 °C, except for the initial shift at high *RH*, both isotherms for CEM I have similar shapes. Due to the fact that our isotherms compare well with H. Ranaivomanana et al. [17] and W. Chen [23], the differences in isotherms with S. Poyet [2] are not attributed to material variability solely. These cannot be attributed either to a kinetics effect: each *RH*-step lasts more than 1200 days in [2]. In terms of microstructure, the batch in [2] displays significantly greater pore sizes and porosity than ours, see Section 3.1: this should lead to lower isotherms than ours, contrarily to what is observed. The most plausible cause for the observed differences is carbonation. Indeed, while we fill our climatic chambers with nitrogen from $RH = 80\%$ and lower, similar to H. Ranaivomanana et al. [17] who do so for all *RH*-steps, S. Poyet [2] takes no specific precaution to avoid carbonation on the sample surfaces. This analysis would deserve further validation, yet it is not the main focus of this contribution.

4. Discussion and analysis

Our results highlight experimentally a thermal activation of desorption isotherms. This observation may be explained by capillary and adsorption theories, using previous studies such as Xi et al. [18].

4.1. Experimental data analysis with capillary theory

4.1.1. Temperature dependence: existence of a master curve?

Capillary theory is used here to assess whether a single master curve exists to describe all the isotherms, whatever the temperature, and possibly also whatever the concrete.

At given temperature T and relative humidity *RH*, capillarity is driven by water chemical potential, which is proportional to $\Re T \ln(RH)$ [11,12]. Former studies on porous non-cementitious materials have shown experimentally that the relationship between the material water retention capacity and water chemical potential does not depend on temperature T, see [12] in the case of starch materials.

Fig. 9(a) plots our experimental data in terms of water content w (%) vs. $\Re T \ln(RH)$. Although several close experimental points are recorded for CEM V concrete at 20 and 50 °C and for CEM I at 50 °C and 80 °C, it is observed that the relationship between w (%) and

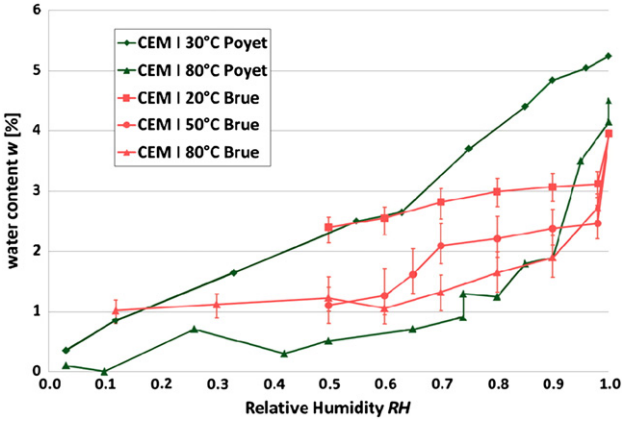

Fig. 8. Comparison of first desorption isotherms (water content w vs. *RH*) of CEM I concrete between this study (labeled 'Brue') and Ref. [2] (labeled 'Poyet'), as a function of temperature.

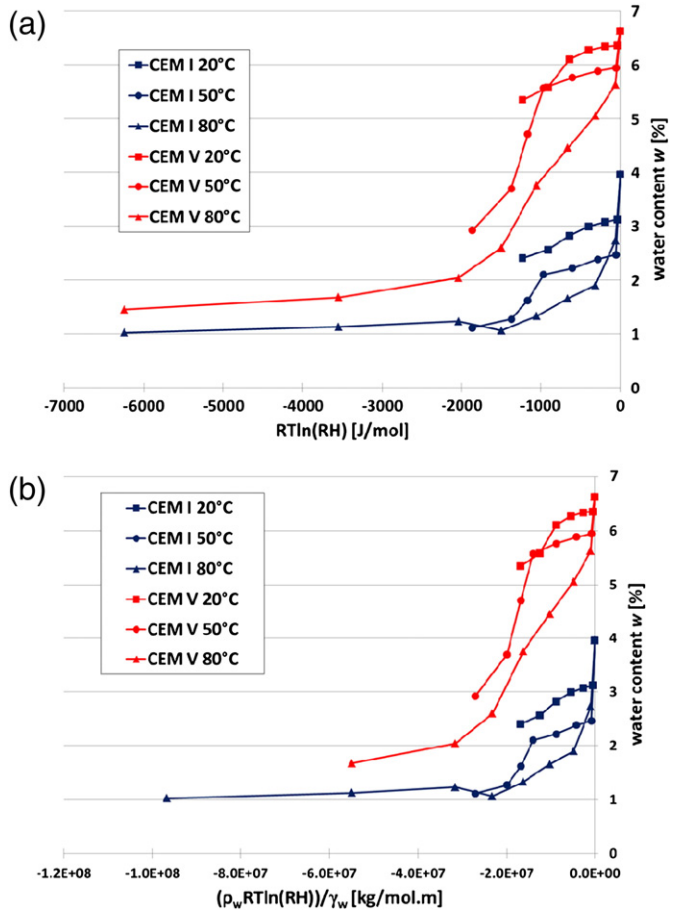

Fig. 9. Water content w (%) of both concretes as a function of temperature T and (a): $\Re T \ln(RH)$ or (b): $\frac{\rho_w \Re T \ln(RH)}{\gamma_w}$.

$\Re T \ln(RH)$ depends on both temperature T and concrete type for $RH \leq 98\%$: no actual master curve can be deduced from this plot.

More rigorously, when capillarity is concerned, temperature T also affects water specific mass ρ_w and surface tension γ_w, see Eq. (1). Indeed, according to Kelvin–Laplace's law, both water chemical potential and $\left(\frac{\rho_w}{\gamma_w}\right)$ are related as follows:

$$\frac{\rho_w \Re T \ln(RH)}{\gamma_w} = -\frac{4M_w}{d^i} \tag{6}$$

where M_w is water molar mass (18 g/mol), and d^i is drained pore diameter, both being no direct function of temperature T. Hence, should capillarity be the main water retention phenomenon, the material water content w would be represented by a single master curve as a function of $\frac{\rho_w \Re T \ln(RH)}{\gamma_w}$. Fig. 9(b) presents the water content w of both concretes as a function of temperature T and $\frac{\rho_w \Re T \ln(RH)}{\gamma_w}$: whatever the concrete considered, no master curve is observed, except for the first two points on the right hand side, which correspond to $RH \geq 98\%$.

From this analysis, it is concluded that, for all temperature levels (20, 50 and 80 °C), variations in capillary pressure are the main desorption mechanism for $RH \geq 98\%$ only.

4.1.2. Use of a simple pore network model

Previous analysis is also supported by the use of a simple pore network model [43]. It is combined with a criterion defining a limit between capillary evaporation and multilayer desorption [44].

4.1.2.1. Description of the pore network model. Herein, the pore network is represented by an array of parallel cylinders of varying

diameter d^i, without interaction with each other and with an identical access to the environment [42,43,45]. A water content repartition, labeled r, is derived from mass variation data at stabilization as:

$$r\left(d^{i+1}\right) = \frac{S_w\left(d^i\right) - S_w\left(d^{i+1}\right)}{\log\left(d^i\right) - \log\left(d^{i+1}\right)} \quad (7)$$

where $S_w(d^i)$ (resp. $S_w(d^{i+1})$) is water saturation level at stabilization at given RH^i (resp. $RH^{i+1}<RH^i$), which corresponds to a smallest drained pore diameter d^i (resp. $d^{i+1}<d^i$). Both d^i and d^{i+1} are assessed using Kelvin–Laplace's equation, see Eq. (1). As Kelvin–Laplace's equation is not defined at $RH=100\%$, pore diameter at $RH=100\%$ is arbitrarily chosen at 500 nm whatever temperature T: this is higher than $d^i(RH=98\%)$ at $T=20$, 50 or 80 °C, see Table 4; also, 500 nm corresponds to negligible intruded pore volume in the pore size distributions given by MIP for both concretes, see Fig. 2: actual pores above 500 nm diameter have a peak size above 1 μm (attributed to micro-cracks or wide interconnected pores), and those below are all the main capillary and nano-pores. Repartition r is interpreted as the mass loss between two neighboring RH values (RH^i and $RH^{i+1}<RH^i$), corresponding to a variation in smallest drained pore diameter from d^i to $d^{i+1}<d^i$. The greater the repartition r between two neighboring diameters $[d^{i+1}; d^i]$, the greater the loss in water content, and so the greater the amount of pores of diameter comprised between $[d^{i+1}; d^i]$.

4.1.2.2. Limit of applicability of the mechanism of capillary evaporation. For varied meso-porous materials such as active charcoals, porous glasses and silica gels, when water is used as the adsorbate, Kadlec et al. [44] validate experimentally a model, which describes the limit in capillary evaporation (towards multilayer desorption) by that of the tensile strength of the water adsorbate. In support to this, all experimental isotherms in [44] display a sharp break, attributed to the transition from capillarity evaporation to desorption, at a relative pressure RH_0 ranging from 37.5 to 50% at ambient temperature. This is associated to characteristic pore radii of 11 to 15.5 Å (i.e. pore diameters of ca. 2.2–3.1 nm). Also, when assuming a water molecule diameter of ca. 3 Å [46–48], a layer of 7 to 10 adsorbed water molecules fills these pores at the limit with multilayer desorption. J. Baron et al. [14] also describe a limit of about ten water molecules in parallel for the transition from capillary evaporation to multilayer desorption.

4.1.2.3. Application to our experimental data. Fig. 10(a) and (b) plots water repartition r vs. drained pore diameter d^i for CEM I and CEM V concretes respectively. For both materials, two distinct peaks in water repartition are observed. The smaller one is on the order of 100 nm, with a value at 100 nm at 20 °C and a lower value at 80 nm at 80 °C for both concretes. Using Kelvin–Laplace's law, this first peak corresponds to $RH\geq 98\%$, whatever T, see Table 4: it is mainly attributed to capillary phenomena.

The second, greater peak in r is centered around 4 nm whatever T for CEM I concrete; it is centered around 4 nm at 20 °C, down to 3 nm at 80 °C for CEM V. The peak shift to smaller drained pores with increasing T is related to thermal activation. This peak has a greater amplitude for CEM V concrete than for CEM I, in relation with the greater amount of nanoscopic pores for CEM V than for CEM I. Also, being within nanoscopic pore sizes, this water loss peak is attributed to multilayer desorption, see above paragraph: pores of ca. 3 to 4 nm, i.e. filled by at most 10–13 water molecules, are bound to be subject to sorption phenomena.

Further, for CEM I concrete, it is observed that water repartition r is more uniformly distributed at 20 and 80 °C than at 50 °C. The greater peak in water loss is observed at 50 °C, for nanoscopic pores, i.e. due to desorption. It is concluded that at 20 and 80 °C, capillarity and desorption contribute similarly to water loss, whereas desorption is predominant at 50 °C. For CEM V concrete, whatever the temperature, the peak for nanoscopic pores is greater than that for capillary pores: desorption is predominant over capillarity as regards water loss. Similarly to CEM I concrete, desorption is most enhanced at 50 °C, where the peak for nanoscopic pores is the greatest.

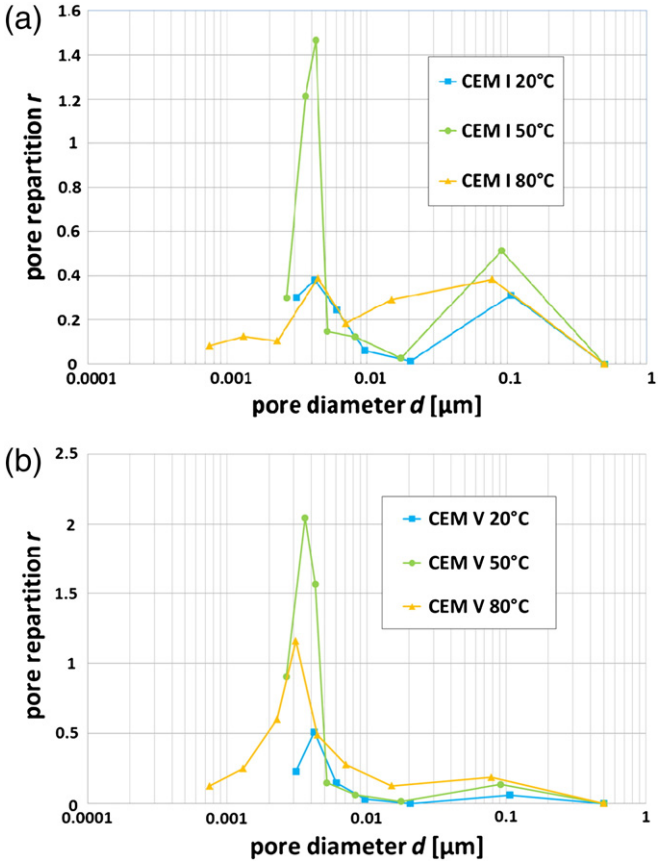

Fig. 10. Water repartition r vs. pore diameter d^i (corresponding to the smallest water drained diameter described by Kelvin–Laplace's law) for (a) CEM I concrete; (b) CEM V concrete.

Finally, for both materials, the area under the curves $r(d^i)$ correspond to the total water loss down to the lowest RH, which increases with temperature. It is observed that this area, limited to pores bigger than 5–7 nm, has a more uniform shape and is greater at $T=80$ °C than for lower temperatures: this is most visible for CEM V concrete. This is attributed to a phenomenon evenly distributed over this pore size range, which is thermally activated above 50 °C. For pores smaller than 5–7 nm i.e. subject to desorption, the area is maximum at 50 °C, as described above.

In brief, at temperatures $T>50$ °C, all along the desorption path, desorption is limited in nanoscopic pores, and water loss is enhanced for bigger pores. At this stage, this may be either due to thermally-enhanced desorption (but then, why should this occur significantly above 50 °C only?), or to a complementary phenomenon, which will be commented upon in Section 4.3. The application of the adsorption BSB model also supports the latter interpretation, as follows.

4.2. Application of a multi-layer adsorption model: the BSB model

4.2.1. Numerical fitting of the isotherms by the BSB model

The BSB model, as described by three parameters C, k and w_m, see Section 1, is fitted at each temperature and for each concrete by a least squares method, by imposing a threshold ε of 10^{-3} (i.e. 0.1%) to the quadratic distance between all experimental data ($RH\in[0;100]$) and numerical prediction. The search for an optimal set $\theta=(C, k, w_m)$

is performed using a Newton algorithm [49], which uses a second order limited development around an initial value of θ. The gradient vector ∇f_θ and the Hessenian matrix $(H_{ij}) = \frac{\partial^2 f_\theta}{\partial\theta^i \partial\theta^j}$ are calculated from Eq. (2) for function $f_\theta(RH) = w(RH)$. The initial value of θ is selected as that minimizing the quadratic distance for all RH values when varying C, k and w_m, each in turn, in the expected range: $C \in [10,50]$; $k \in [0.5;0.9]$; $w_m \in [0.4;8]$, see [18].

Fig. 11(a), (b) and (c) plots both experimental points and optimal numerical fitting at each temperature respectively, for both materials. At 20 °C, very good fitting is obtained for all the experimental points, the greatest distance being obtained at $RH \geq 98\%$. At 50 °C, the fitting displays greater distance to the experimental points: these show a sharp break between 60 and 70%RH, which the model captures only roughly. A more refined model, with a greater number of parameters, would allow closer fitting, yet without the physical interpretation available when using the BSB model. Finally, at 80 °C, a good fitting is obtained, similar to that at 20 °C, except for CEM I at $RH \leq 50\%$ where the fitting consistently underestimates the mass content.

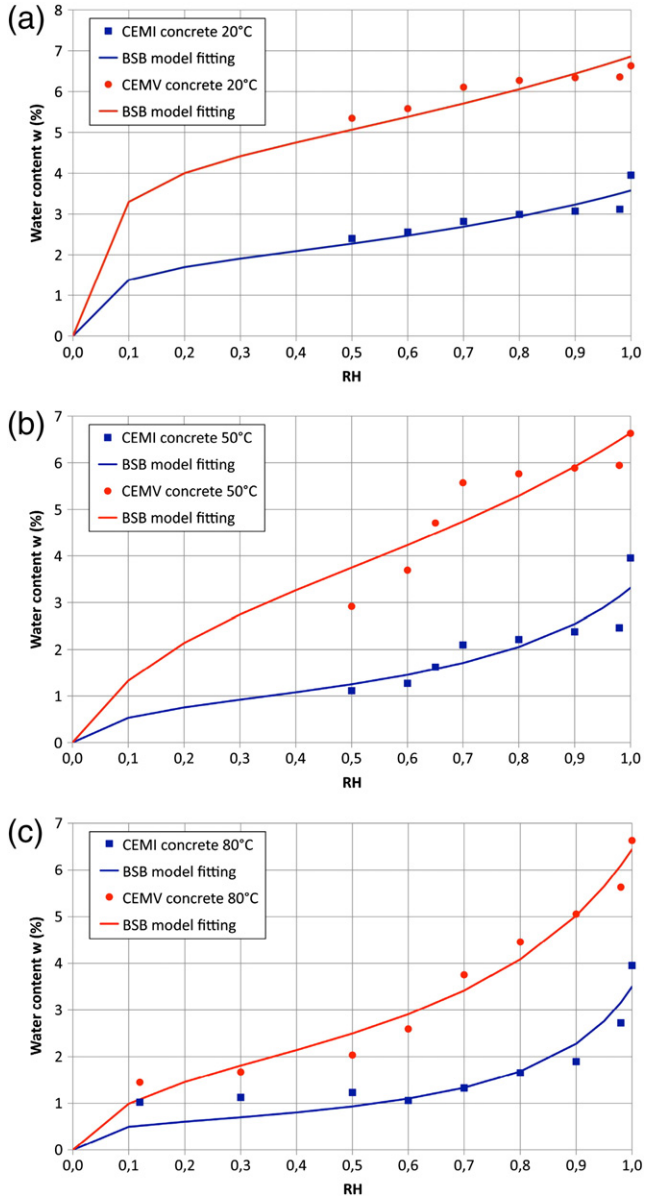

Fig. 11. Comparison between our experimental data and fitting by the BSB model (also named GAB model) for both concretes (a) at 20 °C; (b) at 50 °C; (c) at 80 °C.

Indeed, for this material at 80 °C, one recalls the weight gain at $RH \leq 50\%$, see Fig. 3, which was attributed to temporary failure of the climatic chamber. Hence, the model evolves in the proper direction with a predicted water content lower than that obtained experimentally. As a conclusion, the numerical fitting of our experimental data using the BSB model is adequate. All optimal parameters are provided in Table 5.

4.2.2. Prediction of the number of adsorbed water layers by the BSB model

Xi, Bažant and Jennings [18] propose a physical interpretation of the BSB model parameters, with direct application to Portland cement pastes. No such adequacy is observed for CEM I or CEM V concretes under temperatures $T \leq 80$ °C, as shown below.

In [18], k (<1) is related to the energy necessary for multilayer sorption/desorption. Fitted values show that k is in the adequate range (i.e. <1), and that it increases with increasing temperature T, for both concretes. C is the so-called BET constant, related to the energy released during mono-layer sorption/desorption. C should decrease with temperature T as:

$$C = \exp\left(\frac{E_H - E_L}{\Re T}\right) \tag{8}$$

with E_H (J/mol) total heat of adsorption per mole of vapor, E_L (J/mol) latent heat of condensation per mole and [J/mol·K]. According to Xi et al. [18], the net heat of adsorption writes:

$$(E_H - E_L) = C_0 \tag{9}$$

with $C_0 = 855$ K for water and $T \leq 100$ °C. By fixing C to 18.47 at 20 °C, 14.09 at 50 °C and 11.25 at 80 °C, as derived from Eqs. (8) and (9), no numerical convergence could be achieved. Also, Eq. (8) describes a monotonous decrease in C with increasing T: despite using a rigorous numerical procedure, as detailed above, such evolution could not be achieved with our fitting, see Table 5. Such case is referred to in [18], as being due to the actual complexity of concrete microstructure (with a tortuous pore network, potentially an Interfacial Transition Zone — ITZ [50]), and to unaccounted thermal effects.

Finally, w_m is the mass of water (for 1 g of dried material) needed to complete a mono-molecular adsorbed layer, before switching to multi-layer adsorption. Table 5 shows that fitted w_m values decrease with temperature for both concretes. This means that the amount of water w_m necessary to fill the first layer of adsorbed water at the pore surface decreases with increasing T. This is in accordance with a greater spacing between water molecules, and/or with a greater water molecule diameter (water thermal expansion). Also, w_m values for CEM V are consistently greater than for CEM I, in direct relation with the finer porosity of CEM V, which increases its specific surface, i.e. its sorption capacity.

Moreover, by using a simple rule of proportionality, Eq. (2) may be re-written in terms of a number $n(RH) \propto w(RH)$ of adsorbed water layers:

$$n(RH) = \frac{w(RH)}{w_m} = \frac{C \times k \times RH}{(1 - k \times RH)(1 + (C-1)k \times RH)} \tag{10}$$

Table 5
BSB model parameters fitted by the Newton algorithm [49] for CEM I and CEM V concretes.

	CEM I			CEM V		
	20 °C	50 °C	80 °C	20 °C	50 °C	80 °C
C [–]	50.1	16.3	50.5	67.4	10.0	13.3
k [–]	0.51	0.74	0.84	0.38	0.50	0.73
w_m [%]	1.8	0.87	0.55	4.37	3.65	1.8

By multiplying $n(RH)$ by the diameter of a water molecule (ca. 3 Å), one gets the thickness $t(RH)$ of the adsorbed water layer on the pore walls [17]. Using parameter values from Table 5, $n(RH)$ is calculated from Eq. (10) for both concretes and $T=20$, 50 and 80 °C, see Fig. 12(a) and (b), for CEM I and CEM V respectively. Also, predictions for $n(RH)$ as obtained by S. Poyet [2] for CEM I at 30 and 80 °C are plotted using parameter values provided in [2], see Fig. 12 (a). Firstly, it is observed on both figures that at $RH=100\%$, $n(RH)$ is greater than 1, whatever the concrete and the temperature considered, in good accordance with [18].

As expected, for CEM I, with our fitted parameters, $n(RH)$ decreases with increasing temperature for $T=20$ or 50 °C and $RH\leq 35\%$, see Fig. 12(a): the greater the temperature, the greater the desorption, i.e. the smaller $n(RH)$. Above 35%*RH*, $n(RH)$ increases with increasing temperature, which is against the physical interpretation of this parameter. Also against physical meaning, one observes that $n(RH)$ is consistently greater at 80 °C than at lower temperatures, whatever the *RH*. Parameters fitted by S. Poyet [2] provide a consistently greater number of adsorbed layers $n(RH)$ with increasing temperature, again in contradiction with the physical meaning of this parameter. For CEM V, $n(RH)$ is lower at 50 °C than at 20 °C for $RH\leq 70\%$, whereas it evolves against its expected physical meaning for $RH\geq 70\%$ and $T=80$ °C.

As a conclusion, when using the BSB model, the physical interpretation of $n(RH)=\frac{w(RH)}{w_m}$ as the number of adsorbed water layers holds for $T\leq 50$ °C only, and $RH\leq 35\%$ for CEM I or $RH\leq 70\%$ for CEM V. For higher *RH* (above 35% for CEM I and 70% for CEM V), capillary evaporation, or other phenomena, may be combined to multilayer desorption, so that the BSB model no longer suffices. For $T=80$ °C, this model loses its physical meaning all over the *RH* range, implying that another phenomenon than multilayer desorption alone is at work.

More generally, it is concluded that the BSB model allows a proper three-parameter fitting of water retention properties of both CEM I and CEM V concretes, yet its physical meaning holds only for $RH\leq 35\%$ for CEM I or $RH\leq 70\%$ for CEM V, and $T\leq 50$ °C.

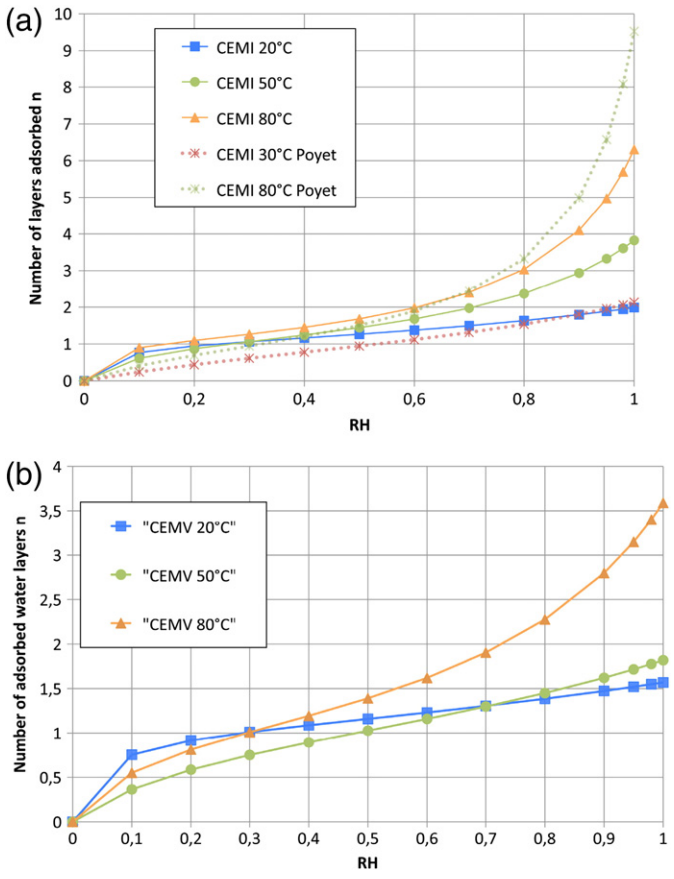

Fig. 12. Plot of the number of adsorbed layers $n(RH,T)=w(RH,T)/w_m$, using the BSB model fitting of (C, k, w_m), for (a): CEMI concrete and (b): CEMV concrete, and comparison with fitted parameters by S. Poyet [2] for CEMI.

4.3. Other influential phenomena: a literature analysis

At this point, in order to account for the inadequate evolution of the BSB model parameters with temperature, we conclude that one (or several) drying mechanisms occur for our concretes above 50 °C, at 80 °C mainly, which act complementarily to adsorption and capillarity. At $T=50$ °C, either capillary evaporation and multilayer desorption are combined or another phenomenon is also at work for $RH\in[35;98]\%$ (for CEM I) or $RH\in[70;98]\%$ (for CEM V). Due to the relative lack of information on the influence of temperature on desorption isotherms [2,4,51], one can make assumptions on several possible mechanisms, from a literature analysis. Following [2], two points are considered as potentially influential for $T\geq 50$ °C: the dehydration of ettringite (and calcium monosulfoaluminate) [52] and the alteration of the C-S-H gel [2].

Ettringite, of chemical formula 3CaO.Al2O3.3CaSO4.32H2O, represents the main AFt phase of hydrated cementitious materials [53]. When present in cement paste, ettringite decomposition may start from as low as 50 °C [54,55]. This decomposition induces calcium monosulfoaluminate formation, which in turn, leads to hydrogarnet and anhydrite formation above 85–90 °C [56,57]. These temperatures are notably modified in the presence of liquid water, see [58]. By using combined TGA and XRD analysis, E. Drouet [36] shows that, at 20 °C, ettringite is present in 3-months old CEM I and CEM V cement pastes. Ettringite is detected at 20 °C, whereas it is significantly decomposed at 50 °C, and remains undetected at 80 °C. Ettringite amounts cannot be quantified separately from TGA experiments, because the decomposition domains of C-S-H and ettringite overlap. Nevertheless, ettringite is replaced by a significant proportion of hydrogarnet (katoïte), which amounts to 0.9 mol/l at 80 °C (to be compared to 0 mol/l at 20 °C). Also, at 20 °C, ettringite decomposes at low *RH* (≤33%) [36]. Albert et al. [52] support the instability of both calcium monosulfoaluminate and ettringite at 25 °C and 1 bar absolute pressure, with decreasing relative humidity (represented by decreasing water chemical potential), owing to thermodynamics calculations. All these elements highlight the unstable nature of ettringite in experimental conditions similar to ours: decreasing *RH* and/or $T=50$ or 80 °C.

Finally, C-S-H may also be impacted by *RH* and temperature variations. It is well-known that C-S-H comprise chemically bound water in varied proportions [53], and that, depending on their packing, Low-Density (LD) and High-Density (HD) C-S-H particles may be distinguished [59]. Aono et al. [60] show that the drying of a hardened cement paste at 50 °C leads to a significant decrease in specific surface area, which is explained by the aggregation of LD C-S-H. Hence, under our experimental thermal conditions ($T\geq 50$ °C), the possible aggregation of LD-C-S-H in the paste may affect desorption isotherms. This interpretation is in good accordance with experimental observations: CEM V contains more C-S-H than CEM I, and, indeed, its desorption isotherms are more affected by temperature increase than CEM I, see Fig. 5. Further research is required to fully validate this interpretation on CEM I and CEM V concretes.

5. Conclusions

In the framework of the French underground disposal for intermediate level/long lived nuclear wastes, we have determined

experimentally the first desorption isotherms of two high performance concretes, CEM I and CEM V (named after their cement type), at constant temperatures T of 20, 50 and 80 °C. The same samples have been followed along their de-saturation path down to 12–60%RH, depending on the temperature. Isotherms at 20 °C have been positively compared to those from two different studies on identical concrete formulations, in order to assess batch variability. Capillary and multilayer desorption models have been fitted to experimental data, and a simple pore network model has provided an estimation of water loss depending on pore size.

The following detailed conclusions are drawn:

- Water retention properties of CEM V are greater than those of CEM I, although CEM V is more porous. This is due to its finer porosity, due to a greater amount of C-S-H than in CEM I.
- CEM V first desorption isotherm is more affected by temperature than CEM I. Again, this is attributed to its greater C-S-H content, which low density (LD) clusters may aggregate at 50 °C and above.
- For both concretes, our isotherms compare well with those of H. Ranaivomanana et al. [17] and W. Chen [23] at 20 °C. Variability due to the difference in concrete batch is not negligible. Moreover, a strong fall in the isotherm at high RH ($\geq$98%) is observed in all three cases; it is more pronounced for CEM I. This quick de-saturation is attributed to the drainage of wide interconnected pores, or of large pores connected by micro-cracks, which are more numerous in CEM I than in CEM V concrete, and which amount also depends on concrete manufacturing (batch).
- Kelvin–Laplace's capillary law is sufficient to describe all isotherms at 20, 50 and 80 °C at high RH ($\geq$98%) only.
- Water loss is plotted against pore size by using a simple pore network model, coupled in first instance with Kelvin–Laplace's law. For both concretes, two peaks in water loss are observed: one is shown to correspond to desorption (the peak in water loss is around 3–4 nm); it is maximal at 50 °C. The other is for capillary evaporation (ca. 80–1000 nm). Also, for $T>50$ °C, all along the de-saturation path, desorption is limited in nanoscopic pores, and water loss enhanced in bigger pores.
- Multilayer desorption is described by the BSB model, which has been extensively validated on cement pastes [18] and concretes [2]. Its rigorous numerical fitting is achieved for all isotherms, for both concretes, to direct use in further numerical modeling. The physical meaning of the BSB model holds only for $RH\leq$35% for CEM I or $RH\leq$70% for CEM V, and $T\leq$50 °C. For $RH\geq$35% (CEM I) or $RH\geq$70% (CEM V) and $T\leq$50 °C, coupled capillary evaporation and multilayer desorption may suffice to describe drying. At $T=$80 °C, a complementary mechanism is bound to occur.
- Complementary mechanisms are suggested from literature analysis. In particular, these are the dehydration of sulfo-aluminate phases (ettringite and calcium mono-sulfo-aluminate), and the aggregation of low density C-S-H, related to C-S-H varying solubility for temperatures lower than 100 °C.

Finally, complementary results of desiccation shrinkage, which were obtained in parallel to desorption isotherms, will possibly help go further on these complex water retention mechanisms. This will be the subject of a forthcoming contribution.

References

[1] ANDRA, Dossier 2005: référentiel des matériaux d'un stockage de déchets à haute activité et à vie longue, Tome 2 : matériaux cimentaires, Document Interne ANDRA n° CRPASCM040015T2_A2005 (in French).
[2] S. Poyet, Experimental investigation of the effect of temperature on the first desorption isotherm of concrete, Cem. Concr. Res. 39 (11) (2009) 1060–1067.
[3] T. Ishida, K. Maekawa, T. Kishi, Enhanced modeling of moisture equilibrium and transport in cementitious materials under arbitrary temperature and relative humidity history, Cem. Concr. Res. 37 (2007) 565–578.
[4] J. Hundt, H. Kantelberg, Sorptionsuntersuchungen an zemeisten, zementmörtel und beton, Deutscher Ausschuss für Stahlbeton Heft, 297, 1978, pp. 25–39.
[5] F. Radjy, E.J. Sellevold, K.K. Hansen, Isosteric vapor pressure–temperature data for water sorption in hardened cement paste: enthalpy, entropy and sorption isotherms at different temperatures, report BYG-DTU R057, Technical University of Denmark (DTU), Lyngby, Denmark, 2003 58 pp.
[6] S. Caré, Effect of temperature on porosity and chloride diffusion in cement pastes, Construct. Build Mater. 22 (2008) 1560–1573.
[7] W.V. Kayser, Temperature dependence of the surface tension water in contact with its saturated vapour, J. Colloid Interface Sci. 56 (1976) 622–627.
[8] M. Jooss, H.W. Reinhardt, Permeability and diffusivity of concrete as function of temperature, Cem. Concr. Res. 32 (2002) 1497–1504.
[9] M. Choinska, A. Khelidj, G. Chatzigeorgiou, G. Pijaudier-Cabot, Effects and interactions of temperature and stress-level related damage on permeability of concrete, Cem. Concr. Res. 37 (1) (2007) 79–88.
[10] S. Poyet, S. Charles, Temperature dependence of the sorption isotherms of cement-based materials: heat of sorption and Clausius–Clapeyron formula, Cem. Concr. Res. 39 (2009) 1060–1067.
[11] J.F. Daïan, Equilibre et transferts en milieux poreux, première partie: Etats d'équilibre, 2010 188 pp. (in French).
[12] P. Westgate, J.Y. Lee, M.R. Ladisch, Modeling of equilibrium sorption of water vapour on starch materials, Am. Soc. Agric. Eng. 35 (1) (1992) 213–219.
[13] J. Baron, R. Sauterey, Le béton hydraulique, Presses de l'Ecole Nationale des Ponts et Chaussées, , 1982 560 pp. (in French).
[14] J. Baron, A. Raharinaivo, Textbook in Civil Engineering for the *Agrégation*, ENS Cachan, France, , 1980–1981 (in French).
[15] IUPAC Recommendations, Pure Appl. Chem. 66 (1994) 1739.
[16] V. Baroghel-Bouny, Water vapour sorption experiments on hardened cementitious materials. Part I: essential tool for analysis of hygral behaviour and its relation to pore structure, Cem. Concr. Res. 37 (3) (2007) 414–437.
[17] H. Ranaivomanana, J. Verdier, A. Sellier, X. Bourbon, Toward a better comprehension and modeling of hysteresis cycles in the water sorption–desorption process for cement based materials, Cem. Concr. Res. 41 (2011) 817–827.
[18] Y. Xi, Z.P. Bažant, H.M. Jennings, Moisture diffusion in cementitious materials–– adsorption isotherms, Adv. Cem. Based Mater. 1 (6) (1994) 248–257.
[19] E.O. Timmermann, Multilayer sorption parameters: BET or GAB values? Colloids Surf. A: Physicochem. Eng. Aspects 220 (2003) 235–260.
[20] S. Brunauer, P.H. Emmett, E. Teller, Adsorption of gases in multimolecular layers, J. Am. Chem. Soc. 60 (2) (1938) 309–319.
[21] S. Brunauer, J. Skalny, E.E. Bodor, Adsorption on nonporous solids, J. Colloid Interface Sci. 30 (1969) 546–552.
[22] F. Benboudjema, F. Meftah, J.M. Torrenti, Interaction between drying, shrinkage, creep and cracking phenomena in concrete, Eng. Struct. 27 (2005) 239–250.
[23] W. Chen, J. Liu, F. Brue, F. Skoczylas, C. A. Davy, X. Bourbon, J. Talandier, Water retention and gas relative permeability of two industrial concretes, Cement and Concrete Research submitted to for publication.
[24] ANDRA, Choix des formulations de référence : ciment CPA-CEM I, caractéristiques mécaniques et de durabilité, Document Interne ANDRA n° C RP 0 CTP 01-002/A, 2001 (in French).
[25] ANDRA, Choix des formulations de bétons de référence, Document Interne ANDRA n° C RP 0 LER 01-004/A, , 2001 (in French).
[26] I. Yurtdas, Couplage comportement mécanique et dessiccation des matériaux à matrice cimentaire : étude expérimentale sur mortier, thèse de doctorat (PhD thesis, in French), Université des Sciences et Technologies de Lille, France, 2003.
[27] N. Burlion, F. Skoczylas, T. Dubois, Induced anisotropic permeability due to drying of concrete, Cem. Concr. Res. 33 (2003) 679–687.
[28] L.J. Klinkenberg, The permeability of porous media to liquid and gas, American Petroleum Institute, Drill. Prod. Prac. (1941) 200–213.
[29] G. Arlaguie, H. Hornain, Grandeurs associées à la Durabilité des Bétons (GranDuBé), Presses de l'Ecole Nationale des Ponts et Chaussées, 2007 437 pp. (in French).
[30] C. Galle, Effect of drying on cement-based materials pore structure as identified by mercury intrusion porosimetry. A comparative study between oven-, vacuum-, and freeze-drying, Cem. Concr. Res. 31 (2001) 1467–1477.
[31] X.-T. Chen, Th. Rougelot, C.A. Davy, W. Chen, F. Agostini, F. Skoczylas, X. Bourbon, Experimental evidence of a moisture clog effect in cement-based materials under temperature, Cem. Concr. Res. 39 (2009) 1139–1148.
[32] Y.F. Houst, Diffusion de gaz, carbonatation et retrait de la pâte de ciment durcie, thèse de l'Ecole Polytechnique Fédérale de Lausanne, , 1992 246 pp. (in French).
[33] A. Korpa, R. Trettin, The influence of different drying methods on cement paste microstructures as reflected by gas adsorption: comparison between freeze-drying (F-drying), D-drying, P-drying and oven-drying methods, Cem. Concr. Res. 36 (2006) 634–649.
[34] S. Mindess, J.F. Young, D. Darwin, Concrete, 2nd Edition Prentice Hall, Englewood Cliffs, NJ, 2002.
[35] P.J. McDonald, V. Rodin, A. Valori, Characterisation of intra- and inter-C-S-H gel pore water in white cement based on an analysis of NMR signal amplitudes as a function of water content, Cem. Concr. Res. 40 (12) (2010) 1656–1663.
[36] E. Drouet, Impact de la température sur la carbonatation des matériaux cimentaires — prise en compte des transferts hydriques. Thèse de Doctorat (PhD Thesis, in French), Ecole Normale Supérieure de Cachan, France, 2010.
[37] R.A. Olson, H.M. Jennings, Estimation of C-S-H content in a blended cement paste using water adsorption, Cem. Concr. Res. 31 (2001) 351–356.
[38] C. Perlot, J. Verdier, M. Carcassès, Influence of cement type on transport properties and chemical degradation: application to nuclear waste storage, Mater. Struct. 39 (2006) 511–523.
[39] S. Kourounis, S. Tsivilis, P.E. Tsakiridis, G.D. Papadimitriou, Z. Tsibouki, Properties and hydration of blended cements with steelmaking slag, Cem. Concr. Res. 37 (2007) 815–822.

[40] A. Lobet, Influence des paramètres de composition des matériaux cimentaires sur les propriétés de transfert, Thèse de doctorat (PhD thesis, in French), INSA de Toulouse, France, 2003.
[41] R.M. Espinosa, L. Franke, Influence of the age and drying process on pore structure and sorption isotherms of hardened cement paste, Cem. Concr. Res. 36 (10) (2006) 1969–1984.
[42] S. Diamond, Mercury porosimetry: an inappropriate method for the measurement of pore size distributions in cement-based materials, Cem. Concr. Res. 30 (2000) 1517–1525.
[43] T. Rougelot, F. Skoczylas, N. Burlion, Water desorption and shrinkage in mortars and cement pastes: experimental study and poromechanical model, Cem. Concr. Res. 39 (2009) 36–44.
[44] O. Kadlec, M.M. Dubinin, Comments on the limit of applicability of the mechanism of capillary condensation, J. Colloid Interface Sci. 31 (4) (1969) 479–489.
[45] R.F. Feldman, P.J. Sereda, A model for hydrated portland cement paste as deduced from sorption-length change and mechanical properties, Mater. Constr. 1 (6) (1968) 509–520.
[46] J. Hagymassy, S. Brunauer, R.S.H. Mikhail, Pore structure analysis by water vapor adsorption I. t-curves for water vapor, J. Colloid Interface Sci. 29 (3) (1969) 485–491.
[47] R. Badmann, N. Stockhausen, M.J. Setzer, The statistical thickness and the chemical potential of adsorbed water films, J. Colloid Interface Sci. 82 (2) (1981) 534–542.
[48] J.A. Odutola, T.R. Dyke, Partially deuterated water dimers: microwave spectra and structure, J. Chem. Phys. 72 (1980) 5062–5070.
[49] J.F. Bonnans, J.C. Gilbert, C. Lemaréchal, C.A. Sagastizábal, Numerical optimization: theoretical and practical aspects, Universitext, Springer-Verlag, Berlin, 2006 (second revised ed. of translation of 1997 French ed.).
[50] J.A. Larbi, Microstructure of the interfacial zone around aggregate particles in concrete, Heron 38 (1) (1993) 1–69.
[51] V. Baroghel-Bouny, M. Mainguy, T. Lassabatère, O. Coussy, Characterization and identification of equilibrium and transfer moisture properties for ordinary and high-performance cementitious materials, Cem. Concr. Res. 29 (1999) 1225–1238.
[52] B. Albert, B. Guy, D. Damidot, Water chemical potential: a key parameter to determine the thermodynamic stability of some hydrated cement phases in concrete? Cem. Concr. Res. 36 (2006) 783–790.
[53] H.F.W. Taylor, Cement Chemistry, Academic Press, London, 1990.
[54] Q. Zhou, F.P. Glasser, Thermal stability and decomposition mechanisms of ettringite at <120 °C, Cem. Concr. Res. 31 (2001) 1333–1339.
[55] M. Castellote, C. Alonso, C. Andrade, X. Turrillas, Composition and microstructural changes of cement pastes upon heating, as studied by neutron diffraction, Cem. Concr. Res. 34 (2004) 1633–1644.
[56] B.A. Clark, P.W. Brown, The formation of calcium sulfoaluminate hydrate compounds: part I, Cem. Concr. Res. 29 (1999) 1943–1948.
[57] B.A. Clark, P.W. Brown, The formation of calcium sulfoaluminate hydrate compounds: part II, Cem. Concr. Res. 30 (2000) 233–240.
[58] V. Baroghel-Bouny, Caractérisation microstructurale et hydrique des pâtes de ciment et des bétons ordinaires et à très hautes performances. Thèse de Doctorat (PhD Thesis, in French), Ecole Nationale des Ponts et Chaussées, Paris, 1994.
[59] H.M. Jennings, A model for the microstructure of calcium silicate hydrates in cement paste, Cem. Concr. Res. 30 (2000) 101–116.
[60] Y. Aono, F. Matsushita, S. Shibata, Y. Hama, Nano-structural changes of C-S-H in hardened cement paste during drying at 50 °C, J. Adv. Concr. Technol. 5 (2007) 313–323.